Peer-reviewed version available at *Nanomaterials* **2019**, *9*, 189; doi:10.3390/nano9020189

Article

Synthesis and Luminescence Properties of Core-Shell-Shell Composites: SiO_2@PMDA-Si-Tb@SiO_2 and SiO_2@PMDA-Si-Tb-phen@SiO_2

Lina Feng [1], Wenxian Li [1,*], Jinrong Bao [1], Yushan Zheng [2], Yilian Li [1], Yangyang Ma [1], Kuisuo Yang [1], Yan Qiao [1] and Anping Wu [1]

[1] Inner Mongolia Key Laboratory of Chemistry and Physics of Rare Earth Materials, School of Chemistry and Chemical Engineering, Inner Mongolia University, Hohhot 010021, China; nmgfln@163.com (L.F.)
[2] Inner Mongolia Autonomous Region Food Inspection Test Center, Hohhot, China; nmgzys@126.com
* Correspondence: nmglwx@163.com (W.L.); Tel: +86-471-4990061

Abstract: Two novel core-shell composites SiO_2@PMDA-Si-Tb, SiO_2@PMDA-Si-Tb-phen with SiO_2 as the core and terbium organic complex as the shell, were successfully synthesized. The terbium ion was coordinated with organic ligand forming terbium organic complex in the shell layer. The bi-functional organosilane $((HOOC)_2C_6H_2(CONH(CH_2)_3Si(OCH_2CH_3)_3)_2$ (abbreviated as PMDA-Si) was used as the first ligand and phen as the second ligand. Furthermore, the silica-modified SiO_2@PMDA-Si-Tb@SiO_2, SiO_2@PMDA-Si-Tb-phen@SiO_2 core-shell-shell composites were also synthesized by sol–gel chemical route. An amorphous silica shell was coated around the SiO_2@PMDA-Si-Tb and SiO_2@PMDA-Si-Tb-phen core-shell composites. The core-shell and core-shell-shell composites both exhibited excellent luminescence in solid state. The luminescence of core-shell-shell composites was stronger than that of core-shell composites. Meanwhile, an improved luminescence stability property for the core-shell-shell composites was found in the aqueous solution. The core-shell-shell composites exhibited bright luminescence, high stability, long lifetime, and good solubility, which may present potential applications in the field of bio-medical.

Keywords: 2,5-bis((3-(triethoxysilyl)propyl)carbamoyl)terephthalic acid (PMDA-Si), core-shell composite; core-shel-shell composite; silica shell; photoluminescence; lifetime

1. Introduction

In the last decade, core-shell composite materials, which connect different functional components integrated into one unit, have attracted increased attention. These materials can be used in many fields, including catalysis [1–7], bio-nanotechnology [8–11], materials chemistry [12,13], optical devices [14–18], electronics [19–22] and magnetic devices [23–27]. Among the number of core-shell composite materials [28–32], coating desirable compounds onto a core to form luminescence materials have emerged as one of the research hot spots in recent years. Compared with unary substance, these core-shell composite materials often exhibit improved physical and chemical properties [33–36], such as good stability, multi-functionality, luminous intensity, fluorescence quantum efficiency, and fluorescence lifetime.

In core-shell composite materials, silicon particles are very important core material because of its aqueous solubility, surface tailorability, low cytotoxicity and low cost [37,38]. Moreover, the surface of silicon particles contains many active free hydroxyl groups and can be chemically bonded to a substance with a functional property. These core-shell composites not only keep core materials stable but also have special shell layer physicochemical properties. So far, there are two commonly

Preprints (www.preprints.org) | NOT PEER-REVIEWED | Posted: 22 January 2019 doi:10.20944/preprints201901.0221.v1

Peer-reviewed version available at Nanomaterials 2019, 9, 189; doi:10.3390/nano9020189

used methods to fabricate core-shell composites. One method is direct precipitation, in which compounds can be deposited on the surface of the SiO_2 core and then form core-shell composites. However, the degree of surface coverage is low and the coating is not uniform. Meanwhile, the prepared composite is unstable and may easily collapse. Another method is silane coupling agent method. Silane coupling agent is a bi-functional organics ($Y(CH_2)_nSiX_3$). Y refers to the organic functional groups, such as amino, carboxyl and double nitrogen. The Y group could coordinate to rare earth ions forming rare earth organic complexes. The X expresses the alkoxy. The Si-O-Si chemical bonds are constructed after the hydrolysis process of X group and the hydroxyl of SiO_2 surface. In such a method, silane coupling agent acted as a "bi-functional molecular bridge molecular" connects SiO_2 spheres and rare earth complexes together. The core-shell composites are stable and the thickness of the shell is easily controlled. Silane coupling agent method is considered as an effective and popular strategy.

There are sufficient researches on core-shell composite materials with SiO_2 as the core and inorganic materials as cladding layer [39–41]. However, the inorganic materials usually exhibited weak luminescence property and restricted their practical application. Therefore, in order to obtain excellent luminescence functional materials, we employed the rare earth organic complexes as the coating layer, which can make full use of the "antenna effect" of organic ligand to achieve higher luminous efficiency [42]. When the rare earth organic complex was fixed on the surface of silica sphere, the non-radiative pathways of high vibration energy loss in the ligand molecules could be largely reduced. In previous work, we have systematically studied the change of luminescence properties of the core-shell composites. Since the thickness of rare earth organic complexes coating layer is nanometer magnitude, it can significantly save the rare earth resources and greatly reduce the production cost [43–46]. These core-shell composites can exhibit excellent luminescence in solid state, however, they usually presented poor luminescent stability properties under aqueous medium. Thus, it is necessary to improve luminescent stability. The silica shell plays an important role on preventing rare earth core-shell composites from quenching of the external environment. In addition, the silica shell can also improve the solubility and luminescent stability of the core-shell composite materials. For example, Ansari et al. prepared hierarchical $CePO_4$:Tb@$LaPO_4$@SiO_2 core-shell-shell composites that had significant application to enhance the solubility, colloidal stability character and luminescence properties [47]. Therefore, the silica-modified sol-gel technique is an ideal option to improve the solubility and luminous stability of rare earth core-shell composites [48]. Such silica coating core-shell composites simultaneously exhibited multi-functionality [49].

In this work, a silane coupling agent method was presented for the synthesis of SiO_2@PMDA-Si-Tb, SiO_2@PMDA-Si-Tb-phen core-shell composites. Specifically, the synthetic approach involved the preparation of organosilane, which acted as a "bi-functional molecular bridge" connecting the silica core and the terbium organic complex shell together by a hydrolysis forming Si–O–Si covalent bonds. Furthermore, the silica-modified SiO_2@PMDA-Si-Tb@SiO_2, SiO_2@PMDA-Si-Tb-phen@SiO_2 core-shell-shell composites were prepared using the TEOS-CTAB sol–gel chemical route. In such a strategy, an amorphous silica shell was successfully coated on the surface of SiO_2@PMDA-Si-Tb and SiO_2@PMDA-Si-Tb-phen core-shell composites. Photoluminescence measurement showed that the core-shell-shell composites SiO_2@PMDA-Si-Tb@SiO_2 and SiO_2@PMDA-Si-Tb-phen@SiO_2 can exhibit good luminescence properties, and stability both in solid state and in aqueous solution medium. These core-shell-shell composite materials with surface-attached abundant Si-OH molecules are easily available for conjugation with biomolecules. Therefore, they could be used for the realistic testing of the biomedical sciences.

Preprints (www.preprints.org) | NOT PEER-REVIEWED | Posted: 22 January 2019 doi:10.20944/preprints201901.0221.v1

Peer-reviewed version available at Nanomaterials 2019, 9, 189; doi:10.3390/nano9020189

2. Materials and Methods

2.1. Material and Reagents

Tb_4O_7 (99.99%), ammonia (25-28%), cetyltrimethylammonium bromide (CTAB, 99%) were all provided by Sigma-Aldrich (Steinheim, Germany). 3-Aminopropyltriethoxysilane (APTES, 99%) was obtained from Acros Organics. Pyromellitic dianhydride (PMDA, 99.2%), 1, 10-phenanthroline (phen, 99%), $Si(OC_2H_5)_4$ (TEOS, 99%) were obtained from Sinopharm Chemical Reagent Co., Ltd. (Shanghai, China). All reagents were analytical grade and used as received without further purification. The terbium perchlorate ($Tb(ClO_4)_3{\cdot}nH_2O$) was prepared by dissolving Tb_4O_7 (99.99%) in $HClO_4$ (1mol L^{-1}) and then evaporated and dried in vacuum.

2.2. Synthesis of Organic Ligand (PMDA-Si)

PMDA-Si was prepared by following the literature method [50,51]. 1 mmol (0.22 g) pyromellitic dianhydride and 25 mL acetone were placed in a 100 mL three-necked round-bottom flask. After the heterogeneous solution was cooled with an ice bath to 0~5 °C, 2 mmol (0.46 mL) APTES was added dropwise. After completion of the addition of the silane, the solution was continually cooled for 2 h and then allowed to stand for 10 h with stirring at room temperature. Then, unreacted acetone was distilled off under reducted pressure. The solid residue was further washed with mineral ether, and then dried under vacuum at 50 °C to obtain PMDA-Si as a white powder. The synthesis route is shown in Figure 1. The resulting PMDA-Si was characterized by ^1H NMR spectrum (Figure S1) and its data is as follows: ^1H-NMR (d_6-DMSO): δ(ppm): 0.61 (4H) | 1.15 (18H) | 1.56 (4H) | 3.33 (4H) | 3.75 (12H) | 7.69 (2H) | 8.48 (2H) | 13.3 (2H)

Elemental analysis $C_{28}H_{48}N_2O_{12}Si_2$:

Calculated C : 50.89 | H : 7.32 | N : 4.24

Found C : 50.80 | H: 7.43 | N : 4.35

Yield: 72.71%.

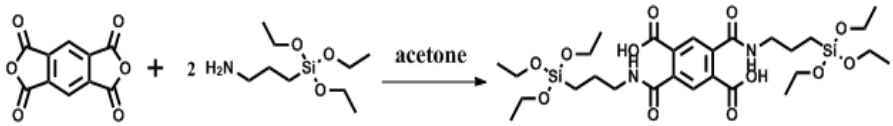

Figure 1. The synthesis route of PMDA-Si.

2.3. Synthesis of Silica Cores

The highly monodisperse silica spheres with size around 178 nm were synthesized by the well-known Stöber process [52]. Typically, 1.7 mL TEOS was rapidly dropped into a mixture that consisted of 40 mL anhydrous ethanol, 4.0 mL deionized water, and 1.7 mL ammonia in a 100 mL single-neck round-bottom flask under vigorously stirred solution. The reaction mixture was then placed in an automatic microwave synthesizer (The pressure was 15 PSI, the power was 150 W, the rotational speed was medium speed and the reaction temperature was 50 °C, respectively.). After 4 h of stirring, the resulting white silica suspension was centrifugally separated and washed with ethanol and deionized water for several times after drying at 50 °C in an oven.

2.4. Synthesis of SiO_2@PMDA-Si

The preparation of SiO_2@PMDA-Si spheres with mass ratio of SiO_2 to PMDA-Si was 10:13. Briefly, 0.20 g SiO_2 spheres were ultrasonically dispersed into 20 mL ethanol forming a homogeneous dispersion, followed by dropwise addition of benzene (30 mL) containing PMDA-Si (0.26 g) under continuous stirring at room temperature. The solution was stirred for 12 h to get a white homogenous mixture. Subsequently, the products were centrifuged, washed thoroughly with anhydrous ethanol successively and repeatedly, and dried in an oven overnight at 50 °C.

Preprints (www.preprints.org) | NOT PEER-REVIEWED | Posted: 22 January 2019 doi:10.20944/preprints201901.0221.v1

Peer-reviewed version available at Nanomaterials 2019, 9, 189; doi:10.3390/nano9020189

2.5. Synthesis of SiO_2@PMDA-Si-Tb and SiO_2@PMDA-Si-Tb-phen

Typically, 0.15 g SiO_2@PMDA-Si spheres were dispersed in 15 mL anhydrous ethanol through ultrasonication. Afterward, 0.07 g $Tb(ClO_4)_3 \cdot nH_2O$ dissolved in 5.0 mL anhydrous ethanol was added dropwise into the above solutions under vigorous stirring. The reaction mixture was heated at 50 °C for 5 h forming a white precipitate. Then resulting white precipitate was collected after centrifugation and dried in an oven overnight at 50 °C. The synthetic procedure for SiO_2@PMDA-Si-Tb-phen was as follows, 0.15 g SiO_2@PMDA-Si spheres and 0.14 g second ligand phen were dispersed in 15 mL anhydrous ethanol through ultrasonication. Then 0.20 g $Tb(ClO_4)_3 \cdot nH_2O$ dissolved in 5.0 mL anhydrous ethanol was slowly added into the above solution under vigorous stirring. The reaction mixture was heated at 50 °C for 5 h. The solution colour changed from white to light pink. Finally, the resulting precipitate was collected by centrifugation and dried in an oven overnight at 50 °C.

2.6. Synthesis of SiO_2@PMDA-Si-Tb@SiO_2 and SiO_2@PMDA-Si-Tb-phen@SiO_2

The Stöber sol-gel technique was popular for silica surface modification. The specific procedure was as follows, the core-shell composite SiO_2@PMDA-Si-Tb or SiO_2@PMDA-Si-Tb-phen (0.03 g), CTAB (0.02 g) and ammonia (0.30 mL) were placed in a 50 mL bottle and well dissolved in a 15 mL mixed solvent of ethanol (7.5 mL) and deionized water (7.5 mL). After stirring the mixture for 10 min at room temperature, 0.03 mL TEOS dissolved in 5.0 mL anhydrous ethanol was added dropwise to the above dispersion to get a white suspension. After continuous stirring for at least 24 h, the final precipitate was separated from the reaction mixture by centrifugation, washed with ethanol, and dried at 50 °C.

2.7. Characterization and Apparatus

^{1}H NMR spectroscopy was performed on a 600 M liquid ^{1}H NMR instrument (Bruker AVANCE III) using DMSO as the solvent and TMS as the internal standard. Elemental analyses were performed with an elemental C, H, N analyzer. The structure and surface morphology of microspheres were studied with scanning electron microscope (SEM, Hitachi S-4800, Japan), and transmission electron microscope (TEM, FEI Tecnai F20, USA) accompanied by energy dispersive X-ray spectroscopy (EDX) to examine the chemical composition. X-ray photoelectron spectroscopy (XPS) was utilized to study surface chemical analysis by Thermo ESCALAB 250Xi spectrometer (Thermo Fisher Scientific, Waltham, MA, USA) with an Al kα radiation source. Thermogravimetric analysis （TGA） was performed on Netzsch STA 409 thermogravimetric analyser at a heating rate of 20 °C min^{-1} under an atmosphere of nitrogen gas. Fourier transform infrared spectra (FT-IR) were measured on a Bruker VERTEX 70 spectrometer at 500-4000 cm^{-1} using the KBr pellet method. X-ray powder diffraction (XRD, RIGAKU, Japan) was measured by a 21 kW extra power X-ray diffractometer using Cu Kα radiation (λ = 1.5406 Å) over an angle range from 5-80°. The photoluminescence spectra and the quantum yields of the solid state products were measured on a photoluminescence spectrometer (FL; Edinburgh S980, UK). The phosphorescence spectra of powder samples were monitored using a FLS980 spectrophotometer at 77 K (FL; Edinburgh S980, UK).

2.8. Lifetime Analysis

The photoluminescence lifetime analysis for the representative emission of Tb^{3+} ions was performed using an Edinburgh FLS980 spectrophotomete at room temperature. The decay curve can be fitted into a biexponential function (1). The lifetime values of the excited state terbium ion ($^5D_4$) could be calculated using the following equation (2), where τ_1 and τ_2 stand for the slow and fast terms of the luminescent lifetime, respectively, and A_1 and A_2 are the corresponding pre-exponential factors.

$$I_{(t)} = I_0 + A_1 \exp(-t_1/\tau_1) + A_2 \exp(-t_2/\tau_2) \quad (1)$$

Preprints (www.preprints.org) | NOT PEER-REVIEWED | Posted: 22 January 2019 doi:10.20944/preprints201901.0221.v1

Peer-reviewed version available at Nanomaterials 2019, 9, 189; doi:10.3390/nano9020189

$$(\tau) = (A_1\tau_1^2 + A_2\tau_2^2)/(A_1\tau_1 + A_2\tau_2) \quad (2)$$

3. Results and Discussion

3.1. The Formation Mechanism and Design Idea of Core-Shell and Core-Shell-Shell Composites

The synthesis strategy for fabricating core–shell and core-shell-shell composites is presented in Scheme 1. It is a key step to synthesize the high surface functionality of silica particles with molecular bridge PMDA-Si. First, the synthetic approach involved the preparation of silica sphere and organosilane PMDA-Si. The PMDA-Si acted as a "bi-functional molecular bridge", and the alkoxyl groups can be covalently bonded with the active hydroxyl groups on the surface of silica spheres forming Si-O-Si bonds. In this process, organosilane PMDA-Si was successfully grafted onto the surface of silica sphere. Thus, the carboxyl group of PMDA-Si could coordinate to terbium ions. Additionally, the introduction of the second ligand phen could also synergistically coordinate to terbium ions by double nitrogen atoms and form terbium organic complex in the shell layer. Here, the core-shell composites were synthesized with SiO_2 as the core and terbium organic complex as the shell. To enhance the solubility and the luminescent stability of the core-shell composite materials, the silica-modified core-shell-shell composites were synthesized. An amorphous silica shell was uniformly coated around these as-prepared core-shell composites by the sol–gel chemical route, which involved the hydrolysis and polycondensation process of TEOS using CTAB as a surface-active agent. As an intermediate layer, the terbium organic complexes were fixed on the inorganic silica substrate. The non-radiative pathways of high vibration energy loss in the ligand molecules could be largely reduced. As a result, it was expected that the emission efficiency of core-shell-shell composites was significantly enhanced. A higher luminescent stability will be obtained under aqueous medium, coming from the protection of an amorphous silica shell.

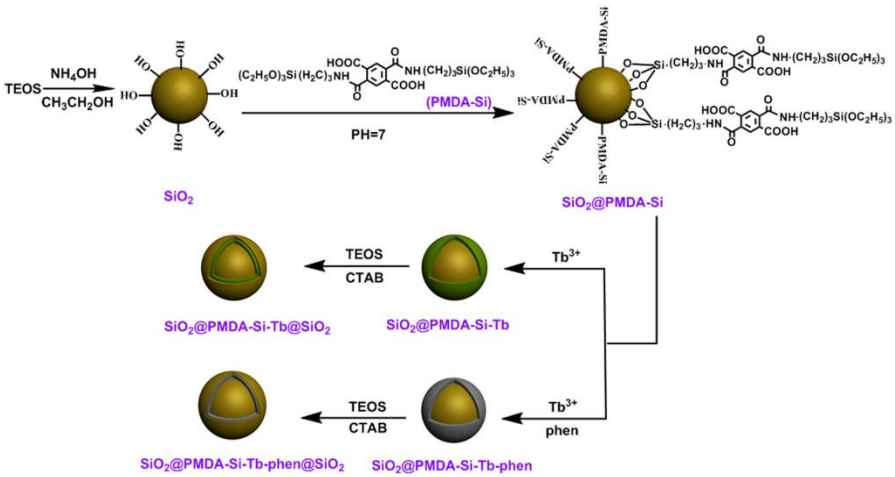

Scheme 1. Schematic illustration of formation mechanism for core-shell and core-shell-shell composites.

3.2. Morphology and Structure

3.2.1. The TEM of SiO_2@PMDA-Si-Tb and SiO_2@PMDA-Si-Tb-phen

The morphological structure and size of the as-prepared SiO_2 are shown in Figure 2a, b. Based on the SEM and TEM micrograph, SiO_2 has a spherical shape and a smooth surface with a mean diameter of around 178 nm. When the functional molecular bridge PMDA-Si was grafted onto the surface of SiO_2, as can be seen with a low-magnification SEM image (Figure 2d), these SiO_2@PMDA-Si particles exhibited perfect uniformity and monodispersity. And the high-magnification TEM image (Figure 2e) indicates that the SiO_2@PMDA-Si particles possess a

Preprints (www.preprints.org) | NOT PEER-REVIEWED | Posted: 22 January 2019 doi:10.20944/preprints201901.0221.v1

Peer-reviewed version available at Nanomaterials 2019, 9, 189; doi:10.3390/nano9020189

relatively rough surface with a mean diameter of 186 nm and thickness of 4 nm. The corresponding histograms of the size distribution are presented in Figure 2c, f.

Simultaneously, the formation of SiO_2@PMDA-Si-Tb and SiO_2@PMDA-Si-Tb-phen core-shell composites was clearly verified by SEM and TEM. Compared with SiO_2@PMDA-Si particles (Figure 2d), the surface morphologies of SiO_2@PMDA-Si-Tb and SiO_2@PMDA-Si-Tb-phen (Figure 3a,d) differed from SiO_2@PMDA-Si sphere. After coated with terbium organic complex layer, the surface of SiO_2@PMDA-Si-Tb and SiO_2@PMDA-Si-Tb-phen core-shell composites became a little larger and much rougher. Figure 3b, c and e, f show the TEM images at the SiO_2@PMDA-Si-Tb and SiO_2@PMDA-Si-Tb-phen core-shell composites, respectively. These core-shell composites were still spherical and nonaggregated, but a slight increase in diameter than the SiO_2@PMDA-Si particles. The changes in diameter were from 178 nm for SiO_2 spheres to 190 nm for SiO_2@PMDA-Si-Tb and SiO_2@PMDA-Si-Tb-phen. It indicated that the terbium organic complexes were coated on the surface of SiO_2 spheres with the thicknesses of about 6 nm. In addition, the element composition of the SiO_2@PMDA-Si-Tb and SiO_2@PMDA-Si-Tb-phen core-shell composites was subsequently analyzed by energy dispersive X-ray spectroscopy (EDX) in Figure 4g, suggested the existence of Si, O, N, Cl and Tb elements in the core-shell composites. These results seem to indicate that the SiO_2@PMDA-Si-Tb and SiO_2@PMDA-Si-Tb-phen core-shell composites were successfully synthesized.

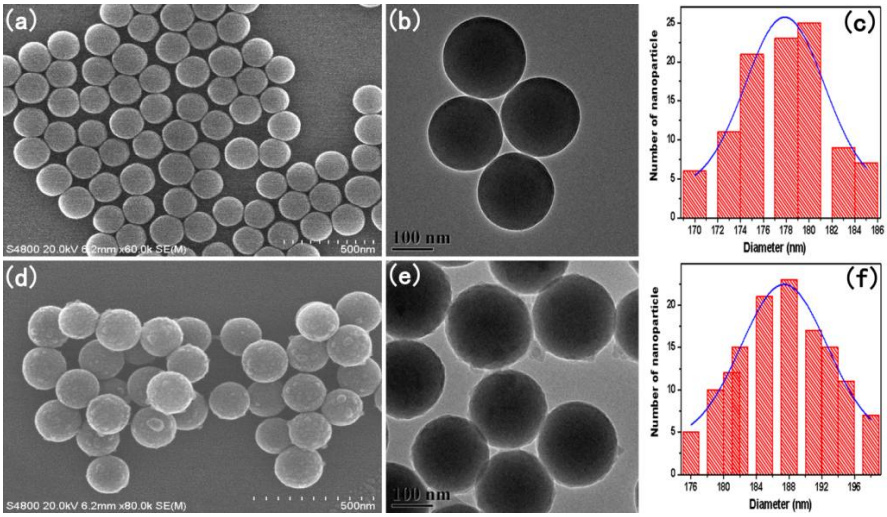

Figure 2. SEM and TEM images of SiO_2 **(a, b)** and SiO_2@PMDA-Si **(d, e)**. Histograms of nanoparticle size distribution of SiO_2 **(c)** and SiO_2@PMDA-Si **(f).**

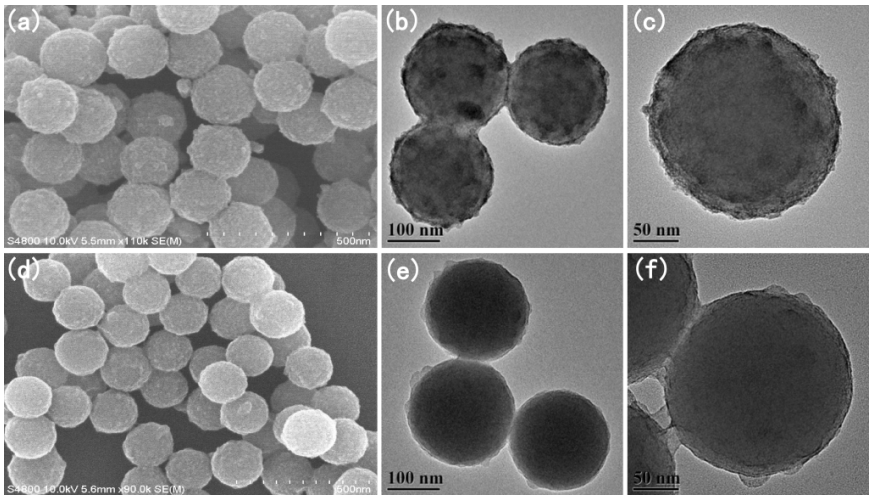

Figure 3. SEM images of SiO_2@PMDA-Si-Tb **(a)** and SiO_2@PMDA-Si-Tb-phen **(d)**; TEM images of SiO_2@PMDA-Si-Tb **(b, c)** and SiO_2@PMDA-Si-Tb-phen **(e, f)**.

Preprints (www.preprints.org) | NOT PEER-REVIEWED | Posted: 22 January 2019 doi:10.20944/preprints201901.0221.v1

Peer-reviewed version available at Nanomaterials 2019, 9, 189; doi:10.3390/nano9020189

3.2.2. The TEM of SiO_2@PMDA-Si-Tb@SiO_2 and SiO_2@PMDA-Si-Tb-phen@SiO_2

In order to widen the application of core-shell composite materials in bio-medical fields, the silica-modified SiO_2@PMDA-Si-Tb@SiO_2, SiO_2@PMDA-Si-Tb-phen@SiO_2 core-shell-shell composites were also synthesized. Further information about the shell growth was provided by TEM analysis. Figure 4a-f shows the TEM images of SiO_2@PMDA-Si-Tb@SiO_2 and SiO_2@PMDA-Si-Tb-phen@SiO_2. There was a clear morphological difference between the SiO_2@PMDA-Si-Tb, SiO_2@PMDA-Si-Tb-phen core-shell composites and the silica-modified SiO_2@PMDA-Si-Tb@SiO_2 (Figure 4a-c), SiO_2@PMDA-Si-Tb-phen@SiO_2 (Figure 4d-f) core-shell-shell composites. Wherein, it showed that the core-shell composites were uniformly encapsulated into a gray shell, and the diameter increased to approximately 210 nm corresponding to a 10 nm thick layer on the surface assigned to amorphous silica. Moreover, the EDX analysis that was performed on the core-shell-shell composites suggested that there still existed the Si, O, N, Cl and Tb elements peaks in the spectrum, however, the Tb content decreased from 15.54% for SiO_2@PMDA-Si-Tb (Figure 4g) to 8.22% for SiO_2@PMDA-Si-Tb@SiO_2 (Figure 4h). Owing to an amorphous silica layer coated onto the surface of SiO_2@PMDA-Si-Tb and SiO_2@PMDA-Si-Tb-phen core-shell composites, eventually causing the reduction of Tb content compared with corresponding core-shell composites. To further confirm the formation of core-shell-shell composite SiO_2@PMDA-Si-Tb@SiO_2, the X-ray elemental mappings analysis was performed. It was clearly showed in the STEM image (Figure 5a) and STEM-EDX elemental mappings (Figure 5b-f) that the elements of N, O, Si, Cl, and Tb were uniformly distributed in the spheres-like area. All the above results indicated the successful preparation of SiO_2@PMDA-Si-Tb@SiO_2 and SiO_2@PMDA-Si-Tb-phen@SiO_2 core-shell-shell composites.

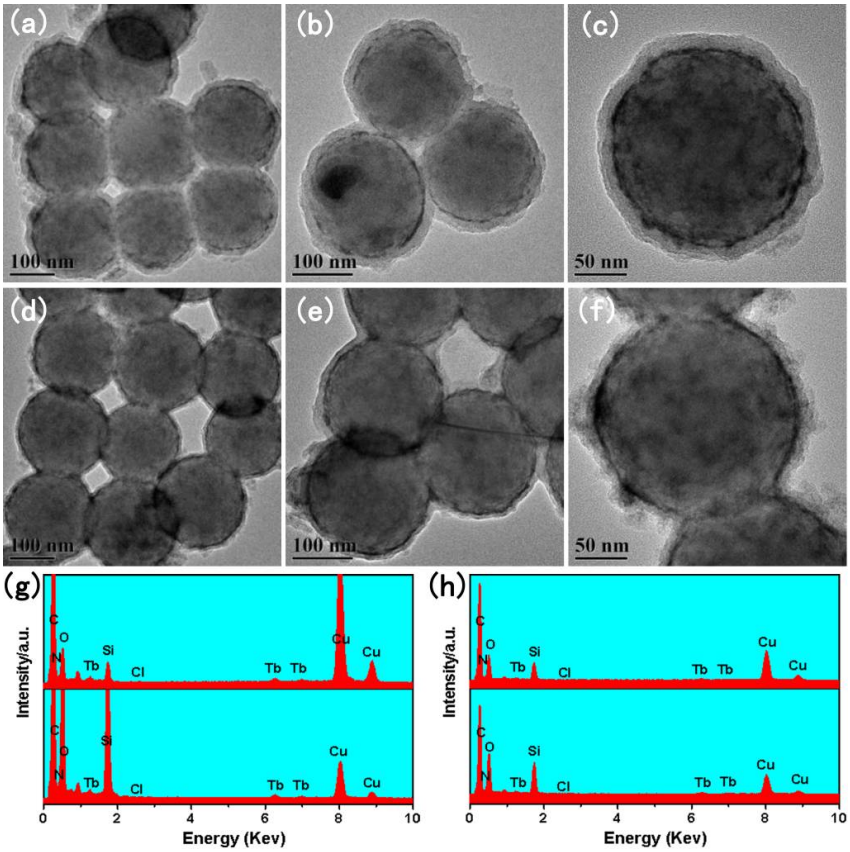

Figure 4. TEM images of SiO_2@PMDA-Si-Tb@SiO_2 **(a-c)** and SiO_2@PMDA-Si-Tb-phen@SiO_2 **(d-f)**; EDX spectra of SiO_2@PMDA-Si-Tb (top panel) **(g)**, SiO_2@PMDA-Si-Tb-phen (bottom panel) **(g)**, and SiO_2@PMDA-Si-Tb@SiO_2 (top panel) **(h)**, SiO_2@PMDA-Si-Tb-phen@SiO_2 (bottom panel) **(h)**.

Preprints (www.preprints.org) | NOT PEER-REVIEWED | Posted: 22 January 2019 doi:10.20944/preprints201901.0221.v1

Peer-reviewed version available at Nanomaterials 2019, 9, 189; doi:10.3390/nano9020189

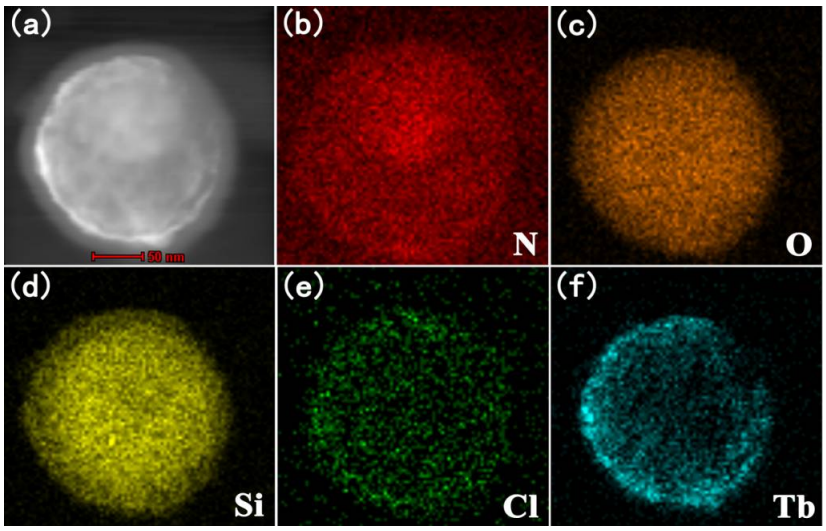

Figure 5. Bright-field STEM image of a single SiO_2@PMDA-Si-Tb@SiO_2 **(a)** and the associated EDX elemental mappings showing the distribution **(b-f)**.

3.3. XPS Analysis

To further explain the incorporation of Tb-(PMDA-Si)-ClO_4 and Tb-(PMDA-Si)-phen-ClO_4 complexes onto the surface of SiO_2, the XPS spectra of PMDA-Si, SiO_2@PMDA-Si-Tb and SiO_2@PMDA-Si-Tb-phen were obtained. As Figure 6a shown, two new peaks at 1240.9 eV and 1274.7 eV appeared after the treatment by Tb^{3+}, and then the existence of Tb^{3+} in the composites can be ascertained. In addition, the corresponding binding energy data for Tb was displayed in Figure 6b. The peaks at around 1240.9 eV and 1274.7 eV indicate the binding energy of Tb $3d_{5/2}$ and $3d_{3/2}$ [53]. On the basis of above analysis, the peaks corresponding to Tb confirmed the successfully incorporation of Tb-(PMDA-Si)-ClO_4 and Tb-(PMDA-Si)-phen-ClO_4 complexes onto the surface of SiO_2.

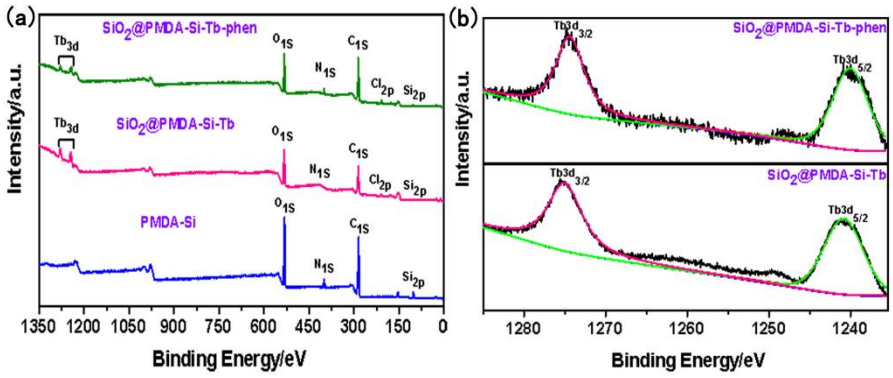

Figure 6. X-ray photoelectron spectroscopic (XPS) analysis of the PMDA-Si, SiO_2@PMDA-Si-Tb and SiO_2@PMDA-Si-Tb-phen samples: XPS full spectra **(a)** and XPS Tb3d spectra **(b)**.

3.4. Thermogravimetric Analysis

The thermal decomposition performance of the synthesized core-shell composite SiO_2@PMDA-Si-Tb-phen and core-shell-shell composite SiO_2@PMDA-Si-Tb-phen@SiO_2 was carried out from ambient temperature to 900 °C under nitrogen atmosphere. As seen in Figure 7, a smaller weight loss in TGA curve exhibits about 2% and 3% for core-shell composite and core-shell-shell composite, respectively, which took place in between 28 and 138 °C. This may be attributed to the evaporation of the surface absorbed water and organic solvents from the sample. Furthermore, the thermal decomposition temperature of core-shell composite SiO_2@PMDA-Si-Tb-phen (Figure 7a) was 160 °C, while it was increased to 200 °C after coating an amorphous silica layer. The thermal

Preprints (www.preprints.org) | NOT PEER-REVIEWED | Posted: 22 January 2019 doi:10.20944/preprints201901.0221.v1

Peer-reviewed version available at Nanomaterials 2019, 9, 189; doi:10.3390/nano9020189

stability of SiO_2@PMDA-Si-Tb-phen@SiO_2 composite (Figure 7b) increases a little due to a growth of silica layer on the surface of SiO_2@PMDA-Si-Tb-phen. A larger weight loss of about 40% and 18% can be seen for the SiO_2@PMDA-Si-Tb-phen and SiO_2@PMDA-Si-Tb-phen@SiO_2 under 650 °C. It can be concluded that the core-shell-shell composite displays higher thermal decomposition temperature, and the core-shell-shell composite has better thermal stability.

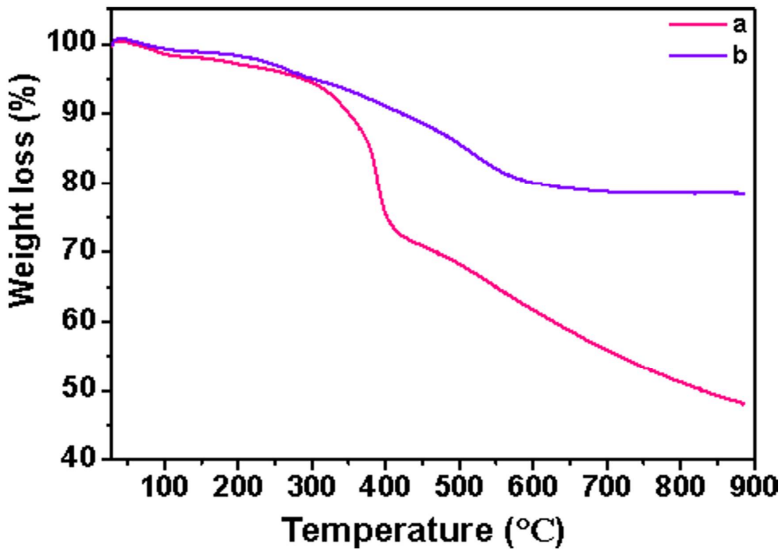

Figure 7. Thermogravimetric analysis curves of the SiO_2@PMDA-Si-Tb-phen **(a)** and SiO_2@PMDA-Si-Tb-phen@SiO_2 **(b)**.

3.5. Infrared Spectra Analysis

3.5.1. The FT-IR Spectra of SiO_2@PMDA-Si-Tb and SiO_2@PMDA-Si-Tb@SiO_2

Further to verify the purity and internal structure of core-shell SiO_2@PMDA-Si-Tb and core-shell-shell SiO_2@PMDA-Si-Tb@SiO_2. The FT-IR spectra of PMDA-Si, SiO_2, SiO_2@PMDA-Si, SiO_2@PMDA-Si-Tb, and SiO_2@PMDA-Si-Tb@SiO_2 are displayed in Figure S2. The appearance of the characteristic bands of PMDA-Si (Figure S2a) at 1633 cm^{-1} and 1550 cm^{-1} was attributed to the stretching vibration of -CONH- bond, and the stretching vibration of -C=O- (COOH) appeared at 1727 cm^{-1}. These characteristic bands demonstrated that functional molecular bridge PMDA-Si had been successfully synthesized through the amidation reaction with pyromellitic dianhydride and 3-aminopropyltriethoxysilane. The band of SiO_2 (Figure S2b) at 1098 cm^{-1} was attributed to the stretching vibration of Si-O-Si group, and Si–OH group was identified at 952 cm^{-1}. In the spectra of SiO_2@PMDA-Si (Figure S2c), the appearance of the characteristic band at 1718 cm^{-1} was ascribed as the stretching vibration of -C=O- (COOH). The characteristic bands at 1641 cm^{-1} and 1556 cm^{-1} were originated from the stretching vibration of -CONH-, which further confirmed the "functional molecular bridge" PMDA-Si onto the surface of SiO_2. The FT-IR spectrum of SiO_2@PMDA-Si-Tb core-shell composites (Figure S2d) shows the characteristic bands of -C=O- (COOH) bonds at 1714 cm^{-1}. There was an obvious change in the absorption band compared with SiO_2@PMDA-Si, indicating that Tb^{3+} ions coordinated to the oxygen atoms of carbonyl group. In addition, observed characteristic infrared band at 1147, 925 and 622 cm^{-1} was assigned to the stretching and bending vibration modes of the perchlorate (ClO_4^-) group. As can be observed in the FT-IR spectrum of the SiO_2@PMDA-Si-Tb@SiO_2 core-shell-shell composites (Figure S2e), there was a significant change between the spectra of SiO_2@PMDA-Si-Tb and SiO_2@PMDA-Si-Tb@SiO_2. After coating the SiO_2 shell, the intensity of the characteristic -CONH- and -C=O-(COOH) absorption bands was obviously decreased. The surface Si-OH groups play an important role for the functionalization and their affinity with bio-molecules, which is usable in the bio-medical field.

Preprints (www.preprints.org) | NOT PEER-REVIEWED | Posted: 22 January 2019 doi:10.20944/preprints201901.0221.v1

Peer-reviewed version available at Nanomaterials 2019, 9, 189; doi:10.3390/nano9020189

3.5.2. The FT-IR Spectra of SiO_2@PMDA-Si-Tb-phen and SiO_2@PMDA-Si-Tb-phen@SiO_2

After further encapsulation by the second ligand phen and SiO_2 shell, the formation process of core-shell and core-shell-shell composites was also investigated by FT-IR spectra. Figure S3a-c shows the FT-IR spectra of phen, SiO_2@PMDA-Si-Tb-phen and SiO_2@PMDA-Si-Tb-phen@SiO_2. Compared the spectra SiO_2@PMDA-Si-Tb-phen (Figure S3b) with SiO_2@PMDA-Si (Figure S2c), the stretching vibration of -C=O- (COOH) red-shifted to 1714 cm^{-1}, and the stretching vibration of -CONH- red-shifted to 1632 cm^{-1} and 1521 cm^{-1}, implying that the -C=O- (COOH) of PMDA-Si was coordinated with Tb^{3+}. Moreover, the stretching vibration of -C=N- in the spectra of free phen (Figure S3a) was located at about 1587 cm^{-1}, however, which had shifted to lower frequencies at 1579 cm^{-1} in the spectra of SiO_2@PMDA-Si-Tb-phen, suggesting that the Tb^{3+} ion coordinated with double nitrogen atoms of phen and Tb-(PMDA-Si)-phen-ClO_4 complexes successfully coated on the surface of SiO_2 core. In the FT-IR spectrum of SiO_2@PMDA-Si-Tb-phen@SiO_2 (Figure S3c), similarly, the intensity of characteristic absorption bands -CONH- and -C=O- (COOH) bonds were obviously decreased, which was deeply indicated that the SiO_2 shell was effectively encapsulated around the surface of SiO_2@PMDA-Si-Tb-phen core-shell composites.

3.6. X-ray Diffraction Analysis

The composition and structure of the powder samples were examined by XRD. Figure 8(A) shows the XRD patterns of SiO_2 core, SiO_2@PMDA-Si, SiO_2@PMDA-Si-Tb and SiO_2@PMDA-Si-Tb@SiO_2, respectively. For SiO_2 directly formed from Stöber method (Figure 8(A)a), there were two broad bands centered at 2θ = 7-8° and 2θ = 23°, which were identical with the standard XRD pattern for amorphous SiO_2. After the bi-functional organosilane PMDA-Si was grafted onto the surface of SiO_2, no other phase was detected from the comparison of SiO_2 in Figure 8(A)b. For SiO_2@PMDA-Si-Tb core-shell composite in Figure 8(A)c, the diffraction pattern also consisted of two broad band appeared at 2θ = 7-8° and 2θ = 23°, and the intensity of the diffraction band became weaker due to the coating of Tb-(PMDA-Si)-ClO_4 complexes. Besides, there were several sharp peaks at about 7.3°, 8.3°, 13.8°, 20.7°, 22.1°, and 23.8°, indicating that Tb-(PMDA-Si)-ClO_4 complexes coated on the surface of SiO_2 core. As illustrated in Figure 8(A)d, the two broad bands of SiO_2@PMDA-Si-Tb@SiO_2 core-shell-shell composites appeared at 2θ = 7-8° and 23° were in coincidence with the stander XRD pattern for SiO_2 core (Figure 8(A)a), which further illustrated that an amorphous SiO_2 was coated onto the surface of SiO_2@PMDA-Si-Tb.

After the incorporation of the phen and SiO_2 shell, the growth of Tb-(PMDA-Si)-phen-ClO_4 and SiO_2 shell onto the core-shell and core-shell-shell composites has been characterized by XRD. Figure 8(B) shows the XRD patterns of SiO_2 core, SiO_2@PMDA-Si, SiO_2@PMDA-Si-Tb-phen and SiO_2@PMDA-Si-Tb-phen@SiO_2. Compared with the diffraction pattern of SiO_2 core (Figure 8(B)a), several small sharp diffraction peaks at about 7.9°, 8.9°, 12.4°, 18.7°, 21.1°, 23.8° and 27° were observed for the SiO_2@PMDA-Si-Tb-phen composites (Figure 8(B)c). It means that the existence of Tb-(PMDA-Si)-phen-ClO_4 on the surface of SiO_2 core. The diffraction pattern of the SiO_2@PMDA-Si-Tb-phen@SiO_2 composites (Figure 8(B)d) displayed the disappearance of several small diffraction peaks. Moreover, the broad bands centered at 2θ = 23° shifted to a little larger diffraction angles compared with the pure SiO_2 core. This phenomenon may be attributed to the growth environment of the silica core and the silica shell was different.

Preprints (www.preprints.org) | NOT PEER-REVIEWED | Posted: 22 January 2019 doi:10.20944/preprints201901.0221.v1

Peer-reviewed version available at Nanomaterials 2019, 9, 189; doi:10.3390/nano9020189

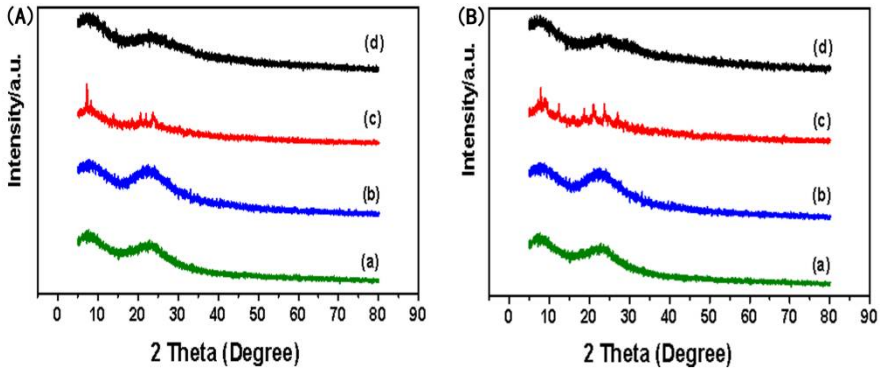

Figure 8. (A) XRD patterns of SiO_2 **(a)**, SiO_2@PMDA-Si **(b)**, SiO_2@PMDA-Si-Tb **(c)** and SiO_2@PMDA-Si-Tb@SiO_2 **(d)**. **(B)** XRD patterns of SiO_2 **(a)**, SiO_2@PMDA-Si **(b)**, SiO_2@PMDA-Si-Tb-phen **(c)** and SiO_2@PMDA-Si-Tb-phen@SiO_2 **(d)**.

3.7. The Photoluminescence Properties

To evaluate the effect of surface modification of SiO_2 on optical absorption properties, photoluminescence spectra were performed to get more information about optical behavior of the Tb(III) core-shell and core-shell-shell composites. As shown in Figure 9, the room temperature fluorescent excitation and emission spectra of core-shell composites SiO_2@PMDA-Si-Tb, SiO_2@PMDA-Si-Tb-phen and core-shell-shell composites SiO_2@PMDA-Si-Tb@SiO_2, SiO_2@PMDA-Si-Tb-phen@SiO_2 were investigated in solid state with the slit width of 1.0 nm.

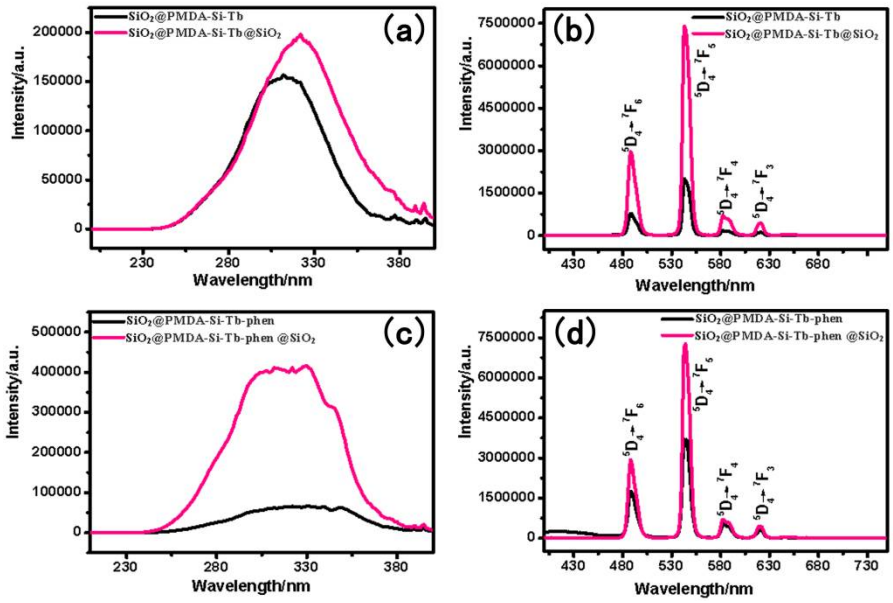

Figure 9. Fluorescent excitation spectra **(a, c)** and emission spectra **(b, d)** of Tb(III) core-shell and core-shell-shell composites (a, b: SiO_2@PMDA-Si-Tb (black line) and SiO_2@PMDA-Si-Tb@SiO_2 (pink line); c, d: SiO_2@PMDA-Si-Tb-phen (black line) and SiO_2@PMDA-Si-Tb-phen@SiO_2 (pink line)).

The excitation spectra monitored at 543 nm were investigated in Figure 9a and c. It can be clearly observed that all excitation spectra exhibited a very broad band at the region of 200–400 nm. The corresponding emission spectra were also measured in Figure 9b and d. These sharp emission peaks at about 488 nm, 543 nm, 583 nm and 621 nm were related to $^5D_4 \rightarrow {}^7F_6$, $^5D_4 \rightarrow {}^7F_5$, $^5D_4 \rightarrow {}^7F_4$ and $^5D_4 \rightarrow {}^7F_3$ transitions of terbium ions, while the $^5D_4 \rightarrow {}^7F_5$ transition at about 543 nm was the strongest [54–56]. Table 1 displays the photoluminescence emission spectra data of the Tb(III) core-shell and core-shell-shell composites. The core-shell composites and core-shell-shell composites both exhibited a much stronger luminescent properties in solid state. Particularly, the core-shell-shell composites displayed stronger luminescence. The strongest emission intensity of

Preprints (www.preprints.org) | NOT PEER-REVIEWED | Posted: 22 January 2019 doi:10.20944/preprints201901.0221.v1

Peer-reviewed version available at Nanomaterials 2019, 9, 189; doi:10.3390/nano9020189

SiO_2@PMDA-Si-Tb@SiO_2 and SiO_2@PMDA-Si-Tb-phen@SiO_2 was 7,420,000 a.u. and 7,314,118 a.u., respectively. Compared with corresponding terbium core-shell composites, the emission intensity of core-shell-shell composites SiO_2@PMDA-Si-Tb@SiO_2 and SiO_2@PMDA-Si-Tb-phen@SiO_2 were about 3.64 and 1.96 times higher. Furthermore, the photoluminescence properties of core-shell and core-shell-shell composites were compared to those of inorganic luminescent material. It is interesting to note that the emission intensities in core-shell and core-shell-shell composites were relatively stronger under the same measurement conditions [57,58]. To further investigate the photoluminescence properties of Tb(III) core-shell and core-shell-shell composites, the absolute quantum yield was determined. The absolute quantum yields of SiO_2@PMDA-Si-Tb and SiO_2@PMDA-Si-Tb-phen were 33.18% and 36.57%, respectively. In contrast, the corresponding absolute quantum yields of SiO_2@PMDA-Si-Tb@SiO_2 and SiO_2@PMDA-Si-Tb-phen@SiO_2 were 41.75% and 47.34%, respectively. When encapsulated with an amorphous silica shell, the core-shell-shell composite materials have a marked increase in absolute quantum yield. These results may be attributed to the fact that non-radiative centers existing on the surface of core-shell composites were eliminated by the shielding effect of the silica shell. It may also result from the suppression of the OH groups quenching effect by the silica shell. Meanwhile, the emission intensities of core-shell-shell composites were significantly enhanced after the coating of an amorphous silica shell. The introduction of the second ligand phen can also synergistically sensitize the luminescence of terbium ions by "antenna effect", and then largely improve the luminescent properties of the core-shell composites.

Table 1. Photoluminescence emission spectra data of the Tb(III) core-shell and core-shell-shell composites.

Composites	Slit Width (nm)	λ_{EX} (nm)	λ_{EM} (nm)	I (a.u.)	Intensity Changes
SiO_2@PMDA-Si-Tb	1.0	312	543	2,040,000	-
SiO_2@PMDA-Si-Tb@SiO_2	1.0	322	543	7,420,000	3.64
SiO_2@PMDA-Si-Tb-phen	1.0	339	543	3,730,000	-
SiO_2@PMDA-Si-Tb-phen@SiO_2	1.0	330	543	7,314,118	1.96

In this work, the luminescence stability of the core-shell composites and core-shell-shell composites in aqueous solution was also studied. The SiO_2@PMDA-Si-Tb, SiO_2@PMDA-Si-Tb-phen and SiO_2@PMDA-Si-Tb@SiO_2, SiO_2@PMDA-Si-Tb-phen@SiO_2 composites were dissolved in deionized water at a concentration of 0.1 g L^{-1}, and were investigated the change of luminescence properties after placed 0, 6, 12, 24, 48 and 72 h with the slit width of 2.0 nm. The aqueous solution was sonicated for 10 min before each measurement to achieve a homogeneous suspension. Figure 10a-d displayed the room temperature fluorescent emission spectra of the composites. It was clearly demonstrated that both the emission spectra of the core–shell and core-shell-shell composites shown four typical peaks at about 488, 543, 583 and 621 nm, which attributed to $^5D_4 \rightarrow {}^7F_6$, $^5D_4 \rightarrow {}^7F_5$, $^5D_4 \rightarrow {}^7F_4$ and $^5D_4 \rightarrow {}^7F_3$ transitions of terbium ions. These results corresponded to the previous study. In addition, with the time increasing from 0 h to 72 h, the decrease degree of emission intensity for core-shell-shell composites were obviously smaller than that for core-shell composites. The core-shell-shell composites exhibited better luminescence stability in the aqueous medium. Especially, the core-shell-shell structure was not collapsed even after three days. The introduction of an amorphous silica shell not only can suppress OH groups quenching effect from the surrounding environment but also can protect the internal structure of the core-shell composites. Therefore, a better luminescent stability in aqueous solution was obtained. This silica-modified core-shell-shell composites, which have been proved to enhance the luminescence efficiency, should be favorable for potential biological application.

Preprints (www.preprints.org) | NOT PEER-REVIEWED | Posted: 22 January 2019 doi:10.20944/preprints201901.0221.v1

Peer-reviewed version available at Nanomaterials 2019, 9, 189; doi:10.3390/nano9020189

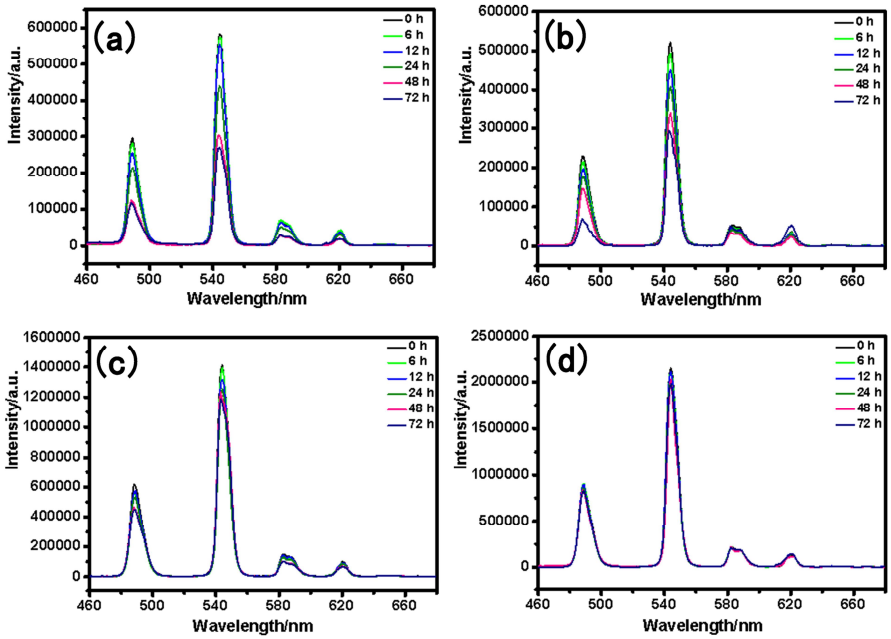

Figure 10. Fluorescent emission spectra of SiO_2@PMDA-Si-Tb **(a)**, SiO_2@PMDA-Si-Tb-phen **(b)**, SiO_2@PMDA-Si-Tb@SiO_2 **(c)** and SiO_2@PMDA-Si-Tb-phen@SiO_2 **(d)** after placement for 0 h, 6 h, 12 h, 24 h, 48 h and 72 h in aqueous solution.

3.8. The Photoluminescence Lifetime

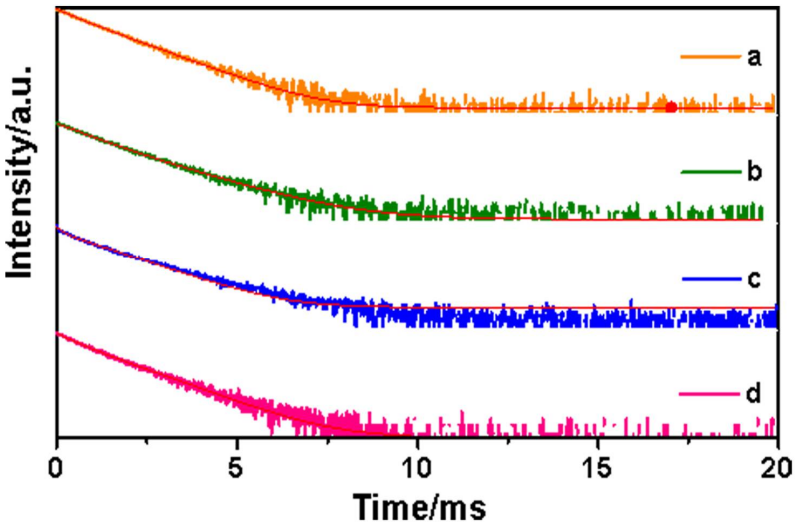

Figure 11. Decay curve of SiO_2@PMDA-Si-Tb **(a)**, SiO_2@PMDA-Si-Tb@SiO_2 **(b)**, SiO_2@PMDA-Si-Tb-phen **(c)** and SiO_2@PMDA-Si-Tb-phen@SiO_2 **(d)**.

In order to study the details of photoluminescence property for terbium core-shell and core-shell-shell composites, the photoluminescence decay curve of SiO_2@PMDA-Si-Tb, SiO_2@PMDA-Si-Tb-phen and SiO_2@PMDA-Si-Tb@SiO_2, SiO_2@PMDA-Si-Tb-phen@SiO_2 composites was recorded in Figure 11. The decay curve can be well fitted into a biexponential function. Herein, calculated average lifetime of two terbium core-shell composites SiO_2@PMDA-Si-Tb and SiO_2@PMDA-Si-Tb-phen were 927.32 μs and 960.85 μs, respectively. Moreover, the average lifetime of two terbium core-shell-shell composites SiO_2@PMDA-Si-Tb@SiO_2 and SiO_2@PMDA-Si-Tb-phen@SiO_2 were 1086.28 μs and 970.18 μs, respectively. The increase of the photoluminescence lifetime for two terbium core-shell-shell composites showed that the quenching from outside particles was strongly reduced after the growth of a silica shell around the core-shell

Preprints (www.preprints.org) | NOT PEER-REVIEWED | Posted: 22 January 2019 doi:10.20944/preprints201901.0221.v1

Peer-reviewed version available at Nanomaterials 2019, 9, 189; doi:10.3390/nano9020189

composites. The detail values are listed in Table 2. Two terbium core-shell-shell composites both have relatively long lifetimes under UV excitation.

Table 2. The lifetime parameters obtained from the biexponential fitting to the photoluminescence decay values of Tb(III) core-shell and core-shell-shell composites.

Composites	A_1	A_2	τ_1 (μs)	τ_2 (μs)	τ (μs)	R^2
SiO_2@PMDA-Si-Tb	620.558	2817.895	409.1	975.2	927.32	0.999
SiO_2@PMDA-Si-Tb-phen	2844.215	1319.362	1009.5	126.9	960.85	0.999
SiO_2@PMDA-Si-Tb@SiO_2	598.777	1044.710	1373.6	805.4	1086.28	0.9999
SiO_2@PMDA-Si-Tb-phen@SiO_2	442.512	1256.689	424.8	1048.2	970.18	0.998

3.9. Low-temperature Phosphorescence Spectra

To verify the intra-molecular energy transfer from the triplet state of the organic ligand to the resonance level of rare earth ion, the phosphorescence spectrum of the first ligand PMDA-Si and second ligand phen was measured under irradiation of 327 nm and 372 nm UV lamp, with slit widths of 1.0 nm and 10.0 nm in the solid state at 77 K (Figure S4). There were two relatively symmetric emission bands between 446 nm and 520 nm in the phosphorescence spectrum of PMDA-Si, just as shown in Figure S4a. The first band ranged from 455 nm to 520 nm, which was defined as T_1. The second band ranged from 446 nm to 454 nm, which was defined as T_2. The triplet state energy level of T_1 was 21978–19231 cm^{-1}, and the triplet state energy level of T_2 was 22422–22026 cm^{-1}. These results suggested that the triplet state energy level of the first ligand PMDA-Si was higher than $^5D_4$ of Tb(III) ions (20430 cm^{-1}) (Figure S4c). Therefore, the first ligand PMDA-Si could effectively transfer the energy absorbed in the ultraviolet region to the central terbium ions by non-radiative transition mode, sensitizing the luminescence of terbium ions. The SiO_2@PMDA-Si-Tb core-shell composites had excellent luminescence.

The phosphorescence spectrum of phen is shown in Figure S4b, there were two phosphorescence emission bands. The first band ranged from 502 nm to 622 nm, which was defined as T_1. The triplet state energy level of T_1 was 19920–16077 cm^{-1}. The second band ranged from 440 nm to 475 nm, which was defined as T_2. The triplet state energy level of T_2 was 22727–21053 cm^{-1}. It was also illustrated that the triplet state energy level of the second ligand phen and the excited state energy of terbium ions matched very well (Figure S4c), and that the second ligand could effectively transfer the energy absorbed in the ultraviolet region to the central terbium ions and sensitize the luminescence of terbium ions. Therefore, according to the low-temperature phosphorescence spectra studies, the organic ligands of PMDA-Si and phen had synergistic reaction to transfer the energy absorbed in the ultraviolet region to the central terbium ions. The photoluminescence intensity of SiO_2@PMDA-Si-Tb-phen was much stronger than the SiO_2@PMDA-Si-Tb core-shell composites.

4. Conclusions

Two novel spherical core-shell composites SiO_2@PMDA-Si-Tb and SiO_2@PMDA-Si-Tb-phen were successfully synthesized with organosilane PMDA-Si acting as a "bi-functional molecular bridge". Moreover, silica-modified SiO_2@PMDA-Si-Tb@SiO_2 and SiO_2@PMDA-Si-Tb-phen@SiO_2 core-shell-shell composites were also successfully synthesized. The formation mechanism of core-shell and core-shell-shell composite was proposed. The TEM and STEM images showed that

the terbium organic complex was successfully coated on the surface of SiO_2 spheres and the amorphous silica shell was uniformly encapsulated around these as-prepared core-shell composites. The core-shell and core-shell-shell composites both exhibited a much stronger luminescent properties in solid state. The photoluminescence emission intensity of SiO_2@PMDA-Si-Tb@SiO_2 and SiO_2@PMDA-Si-Tb-phen@SiO_2 was about 3.64 and 1.96 times higher compared with the homologous terbium core-shell composites. By coating a silica shell on the surface of core-shell composites, better luminescence property and stability for SiO_2@PMDA-Si-Tb@SiO_2 and SiO_2@PMDA-Si-Tb-phen@SiO_2 were found in the aqueous medium. In the core-shell-shell composite materials, the cheap silica was used as supporting cores and the nanometer magnitude terbium organic complex was employed as coating layers, which could significantly save rare earth resources and reduce the production cost. In sum, the whole synthesis procedure of the core-shell-shell composites was quite facile and easy to scale up, which has great potential for low-cost commercial applications.

Supplementary Materials: The following are available online at www.mdpi.com/xxx/s1, Figure S1: The ^{1}HNMR of PMDA-Si; Figure S2: FT-IR spectra of PMDA-Si, SiO_2, SiO_2@PMDA-Si, SiO_2@PMDA-Si-Tb, and SiO_2@PMDA-Si-Tb@SiO_2; Figure S3: FT-IR spectra of phen, SiO_2@PMDA-Si-Tb-phen, and SiO_2@PMDA-Si-Tb-phen@SiO_2; Figure S4: Phosphorescence spectra of PMDA-Si and phen, Triplet state of PMDA-Si, phen and the excited state of Tb(III);

Author Contributions: conceptualization, W.L. and L.F.; methodology, W.L.; software, L.F.; validation, W.L., Y.Z. and J.B.; formal analysis, L.F.; investigation, L.F.; resources, L.F.; data curation, Y.L., Y.M., K.Y. and A.W.; writing—original draft preparation, L.F.; writing—review and editing, W.L., J.B. and Y.Q.; visualization, L.F.; supervision, W.L.; project administration, W.L.; funding acquisition, W.L. All authors have read and approved the final version.

Funding: This research was funded by the Major projects of Natural Science Foundations of Inner Mongolia Science Foundation (No. 2015ZD01) and the Natural Science Foundations of Inner Mongolia Science Foundation (No. 2015MS0502).

Conflicts of Interest: The authors declare no conflict of interest.

References

1. Lu, A.H.; Salabas, E.L.; Schüth, F. Magnetic nanoparticles: Synthesis, protection, functionalization, and application. *Angew. Chemie - Int. Ed.* **2007**, *46*, 1222–1244.
2. Gawande, M.B.; Rathi, A.K.; Nogueira, I.D.; Varma, R.S.; Branco, P.S. Magnetite-supported sulfonic acid: A retrievable nanocatalyst for the Ritter reaction and multicomponent reactions. *Green Chem.* **2013**, *15*, 1895–1899.
3. Gawande, M.B.; Branco, P.S.; Varma, R.S. Nano-magnetite (Fe_3O_4) as a support for recyclable catalysts in the development of sustainable methodologies. *Chem. Soc. Rev.* **2013**, *42*, 3371–3393.
4. Gawande, M.B.; Bonifácio, V.D.B.; Varma, R.S.; Nogueira, I.D.; Bundaleski, N.; Ghumman, C.A.A.; Teodoro, O.M.N.D.; Branco, P.S. Magnetically recyclable magnetite-ceria (Nanocat-Fe-Ce) nanocatalyst-applications in multicomponent reactions under benign conditions. *Green Chem.* **2013**, *15*, 1226–1231.
5. Astruc, D.; Daniel, M.-C. Gold Nanoparticles: Assembly, Supramolecular Chemistry, Quantum-Size-Related Properties, and Applications toward Biology, Catalysis, and Nanotechnology. *Chem. Rev.* **2004**, *104*, 293–346.
6. Purbia, R.; Paria, S. Yolk/shell nanoparticles: Classifications, synthesis, properties, and applications. *Nanoscale* **2015**, *7*, 19789–19873.
7. Duan, S.; Du, Z.; Fan, H.; Wang, R. Nanostructure Optimization of Platinum-Based Nanomaterials for Catalytic Applications. *Nanomaterials* **2018**, *8*, 949.
8. Ow, H.; Larson, D.R.; Srivastava, M.; Baird, B.A.; Webb, W.W.; Wiesnert, U. Bright and stable core-shell fluorescent silica nanoparticles. *Nano Lett.* **2005**, *5*, 113–117.
9. Zhang, F.; Braun, G.B.; Shi, Y.; Zhang, Y.; Sun, X.; Reich, N.O.; Zhao, D.; Stucky, G. Fabrication of Ag@SiO_2@Y_2O_3 : Er Nanostructures for Bioimaging : Tuning of the Upconversion Fluorescence with Silver Nanoparticles -- Supporting Info. *J. Am. Chem. Soc.* **2010**, *132*, 2850–2851.

10. Laurent, S.; Forge, D.; Port, M.; Roch, A.; Robic, C.; Vander Elst, L.; Muller, R.N. Magnetic Iron Oxide Nanoparticles: Synthesis, Stabilization, Vectorization, Physicochemical Characterizations, and Biological Applications. *Chem. Rev.* **2008**, *108*, 2064–2110.
11. Gong, X.; Peng, S.; Wen, W.; Sheng, P.; Li, W. Design and fabrication of magnetically functionalized core/shell microspheres for smart drug delivery. *Adv. Funct. Mater.* **2009**, *19*, 292–297.
12. Fredin, L.A.; Li, Z.; Ratner, M.A.; Lanagan, M.T.; Marks, T.J. Enhanced energy storage and suppressed dielectric loss in oxide core-shell-polyolefin nanocomposites by moderating internal surface area and increasing shell thickness. *Adv. Mater.* **2012**, *24*, 5946–5953.
13. Xu, Z.; Zhang, L.; Mei, B.; Tu, J.; Wang, R.; Chen, M.; Cheng, Y. A Rapid Surface-Enhanced Raman Scattering (SERS) Method for Pb^{2+} Detection Using L-Cysteine-Modified Ag-Coated Au Nanoparticles with Core–Shell Nanostructure. *Coatings* **2018**, *8*, 394.
14. Yin, D.; Wang, C.; Ouyang, J.; Zhang, X.; Jiao, Z.; Feng, Y.; Song, K.; Liu, B.; Cao, X.; Zhang, L.; et al. Synthesis of a novel core-shell nanocomposite Ag@SiO_2@Lu_2O_3:Gd/Yb/Er for large enhancing upconversion luminescence and bioimaging. *ACS Appl. Mater. Interfaces* **2014**, *6*, 18480–18488.
15. Polido Legaria, E.; Saldan, I.; Svedlindh, P.; Wetterskog, E.; Gunnarsson, K.; Kessler, V.G.; Seisenbaeva, G.A. Coordination of rare earth element cations on the surface of silica-derived nanoadsorbents. *Dalt. Trans.* **2018**, *47*, 1312–1320.
16. Myroshnychenko, V.; Rodríguez-Fernández, J.; Pastoriza-Santos, I.; Funston, A.M.; Novo, C.; Mulvaney, P.; Liz-Marzán, L.M.; García De Abajo, F.J. Modelling the optical response of gold nanoparticles. *Chem. Soc. Rev.* **2008**, *37*, 1792–1805.
17. Yu, X.; Wan, J.; Shan, Y.; Chen, K.; Han, X. A facile approach to fabrication of bifunctional magnetic-optical Fe_3O_4@ZnS microspheres. *Chem. Mater.* **2009**, *21*, 4892–4898.
18. Wang, L.; Clavero, C.; Huba, Z.; Carroll, K.J.; Carpenter, E.E.; Gu, D.; Lukaszew, R.A. Plasmonics and enhanced magneto-optics in core-shell Co-Ag nanoparticles. *Nano Lett.* **2011**, *11*, 1237–1240.
19. Georgakilas, V.; Bourlinos, A.B.; Zboril, R.; Steriotis, T.A.; Dallas, P.; Stubos, A.K.; Trapalis, C. Organic functionalisation of graphenes. *Chem. Commun.* **2010**, *46*, 1766–1768.
20. Georgakilas, V.; Otyepka, M.; Bourlinos, A.B.; Chandra, V.; Kim, N.; Kemp, K.C.; Hobza, P.; Zboril, R.; Kim, K.S. Functionalization of graphene: Covalent and non-covalent approaches, derivatives and applications. *Chem. Rev.* **2012**, *112*, 6156–6214.
21. Pykal, M.; Šafářova, K.; Siškova, K.M.; Jurečka, P.; Bourlinos, A.B.; Zbořil, R.; Otyepk, M. Lipid enhanced exfoliation for production of graphene nanosheets. *J. Phys. Chem. C* **2013**, *117*, 11800–11803.
22. Zbořil, R.; Karlický, F.; Bourlinos, A.B.; Steriotis, T.A.; Stubos, A.K.; Georgakilas, V.; Šafářová, K.; Jančík, D.; Trapalis, C.; Otyepka, M. Graphene fluoride: A stable stoichiometric graphene derivative and its chemical conversion to graphene. *Small* **2010**, *6*, 2885–2891.
23. Zhao, L.; Liu, H.; Wang, F.; Zeng, L. Design of yolk-shell Fe_3O_4@PMAA composite microspheres for adsorption of metal ions and pH-controlled drug delivery. *J. Mater. Chem. A* **2014**, *2*, 7065–7074.
24. Ding, H.L.; Zhang, Y.X.; Wang, S.; Xu, J.M.; Xu, S.C.; Li, G.H. Fe_3O_4@SiO_2 core/shell nanoparticles: The silica coating regulations with a single core for different core sizes and shell thicknesses. *Chem. Mater.* **2012**, *24*, 4572–4580.
25. Zou, R.; Gong, S.; Shi, J.; Jiao, J.; Wong, K.L.; Zhang, H.; Wang, J.; Su, Q. Magnetic-NIR Persistent Luminescent Dual-Modal ZGOCS@MSNs@Gd_2O_3 Core-Shell Nanoprobes for in Vivo Imaging. *Chem. Mater.* **2017**, *29*, 3938–3946.
26. Peng, D.L.; Hihara, T.; Sumiyama, K.; Morikawa, H. Structural and magnetic characteristics of monodispersed Fe and oxide-coated Fe cluster assemblies. *J. Appl. Phys.* **2002**, *92*, 3075–3083.
27. She, H.; Chen, Y.; Chen, X.; Zhang, K.; Wang, Z.; Peng, D.L. Structure, optical and magnetic properties of Ni@Au and Au@Ni nanoparticles synthesized via non-aqueous approaches. *J. Mater. Chem.* **2012**, *22*, 2757–2765.
28. Park, H.H.; Woo, K.; Ahn, J.P. Core-shell bimetallic nanoparticles robustly fixed on the outermost surface of magnetic silica microspheres. *Sci. Rep.* **2013**, *3*, 1–7.
29. Amouri, H.; Desmarets, C.; Moussa, J. Confined nanospaces in metallocages: Guest molecules, weakly encapsulated anions, and catalyst sequestration. *Chem. Rev.* **2012**, *112*, 2015–2041.
30. Wang, H.; Chen, L.; Feng, Y.; Chen, H. Exploiting core-shell synergy for nanosynthesis and mechanistic investigation. *Acc. Chem. Res.* **2013**, *46*, 1636–1646.

31. Wang, B.; Zhu, X.; Li, S.; Chen, M.; Lu, H.; Yang, Y. Ag@SiO_2 Core-shell Nanoparticles Embedded in a TiO_2 Mesoporous Layer Substantially Improve the Performance of Perovskite Solar Cells. *Nanomaterials* **2018**, *8*, 701.
32. Kukułka, W.; Wenelska, K.; Baca, M.; Chen, X.; Mijowska, E. From Hollow to Solid Carbon Spheres: Time-Dependent Facile Synthesis. *Nanomaterials* **2018**, *8*, 861.
33. Jiang, H.L.; Akita, T.; Ishida, T.; Haruta, M.; Xu, Q. Synergistic catalysis of Au@Ag core-shell nanoparticles stabilized on metal-organic framework. *J. Am. Chem. Soc.* **2011**, *133*, 1304–1306.
34. Douvalis, A.P.; Zboril, R.; Bourlinos, A.B.; Tucek, J.; Spyridi, S.; Bakas, T. A facile synthetic route toward air-stable magnetic nanoalloys with Fe-Ni/Fe-Co core and iron oxide shell. *J. Nanoparticle Res.* **2012**, *14*.
35. Maity, D.; Zoppellaro, G.; Sedenkova, V.; Tucek, J.; Safarova, K.; Polakova, K.; Tomankova, K.; Diwoky, C.; Stollberger, R.; MacHala, L.; et al. Surface design of core-shell superparamagnetic iron oxide nanoparticles drives record relaxivity values in functional MRI contrast agents. *Chem. Commun.* **2012**, *48*, 11398–11400.
36. Pang, X.; Zhao, L.; Han, W.; Xin, X.; Lin, Z. A general and robust strategy for the synthesis of nearly monodisperse colloidal nanocrystals. *Nat. Nanotechnol.* **2013**, *8*, 426–431.
37. Zou, H.; Wu, S.; Shen, J. Polymer/Silica Nanocomposites: Preparation, Characterization, Properties, and Applications. *Chem. Rev.* **2008**, *108*, 3893–3957.
38. Guerrero-Martínez, A.; Pérez-Juste, J.; Liz-Marzán, L.M. Recent progress on silica coating of nanoparticles and related nanomaterials. *Adv. Mater.* **2010**, *22*, 1182–1195.
39. Lee, H.J.; Park, J.U.; Choi, S.; Son, J.; Oh, M. Synthesis and photoluminescence properties of Eu^{3+}-doped silica@coordination polymer core-shell structures and their calcinated silica@Gd_2O_3:Eu and hollow Gd_2O_3:Eu microsphere products. *Small* **2013**, *9*, 561–569.
40. Tseng, T.K.; Choi, J.; Davidson, M.; Holloway, P.H. Synthesis and luminescent characteristics of europium dopants in SiO_2/Gd_2O_3 core/shell scintillating nanoparticles. *J. Mater. Chem.* **2010**, *20*, 6111–6115.
41. Shibata, H.; Imakita, K.; Fujii, M. Fabrication of a core-shell-shell particle with a quarter-wave thick shell and its optical properties. *RSC Adv.* **2014**, *4*, 32293–32297.
42. Sabbatini, N.; Guardigli, M.; Lehn, J.-M. Luminescent lanthanide complexes as photochemical supramolecular devices. *Coordination Chemistry Reviews*, **1993**, *123*, 201–228.
43. Yang, K.S.; Li, Y.L.; Ma, Y.Y.; Feng, L.N.; Wu, A.P.; Qiao, Y.; Bao, J.R.; Li, W.X.; Zhu, X.W.; Yu, R.B. Synthesis and photoluminescence properties of novel core–shell–shell SiO_2@$CePO_4$:Tb@SiO_2 submicro-spheres. *CrystEngComm* **2018**, *20*, 6351–6357.
44. Li, W.X.; Zheng, Y.S.; Cao, X.F.; Bai, J.; Fu, Z.F.; Bao, J.R.; Li, Y.L. Preparation, characterization, and luminescence properties of dysprosium perchlorate with MABA-Si and phen or dipy complexes as well as SiO_2@Dy(MABA-Si)L core-shell structure nanometermeter luminescent composites. *J. Lumin.* **2016**, *178*, 470–478.
45. Ma, Y.; Li, W.; Zheng, Y.; Bao, J.; Li, Y.; Feng, L.; Yang, K. Preparation , characterization and luminescence properties of core–shell ternary terbium composites $SiO_{2(600)}$@Tb(MABA-Si)L. *R. Soc. open sci.* **2018**, *5*, 171655.
46. Fu, Z.F.; Li, W.X.; Bai, J.; Bao, J.R.; Cao, X.F.; Zheng, Y.S. Synthesis, characterization and luminescence of europium perchlorate with MABA-Si complex and coating structure SiO_2@Eu(MABA-Si) luminescence nanoparticles. *Luminescence* **2017**, *32*, 327–333.
47. Ansari, A.A. Silica-modified luminescent $LaPO_4$:Eu@$LaPO_4$@SiO_2 core/shell nanorods: Synthesis, structural and luminescent properties. *Luminescence* **2018**, *33*, 112–118.
48. Petrov, A.; Lehmann, H.; Finsel, M.; Klinke, C.; Weller, H.; Vossmeyer, T. Synthesis and Characterization of Monodisperse Metallodielectric SiO_2@Pt@SiO_2 Core-Shell-Shell Particles. *Langmuir* **2016**, *32*, 848–857.
49. Zhang, J.; Liu, F.; Li, T.; He, X.; Wang, Z. Surface charge effect on the cellular interaction and cytotoxicity of $NaYF_4$:Yb^{3+}, Er^{3+}@SiO_2 nanoparticles. *RSC Adv.* **2015**, *5*, 7773–7780.
50. Pfeifer, S.; Schwarzer, A.; Schmidt, D.; Brendler, E.; Veith, M.; Kroke, E. Precursors for pyromellit-bridged silica sol-gel hybrid materials. *New J. Chem.* **2013**, *37*, 169–180.
51. Pfeifer, S.; Brendler, E.; Veith, M.; Kroke, E. Hybrid-coatings derived from pyromellitic acid bridged alkoxy-silylalkyl precursors. *J. Sol-Gel Sci. Technol.* **2014**, *70*, 191–202.
52. Stöber, W.; Fink, A. Controlled Growth of Monodisperse Silica Spheres in the Micron Size Range. *J. Colloid Interface Sci.* **1968**, *26*, 62–69.

53. Ji, G.; Gao, X.; Zheng, T.; Guan, W.; Liu, H.; Liu, Z. Postsynthetic Metalation Metal-Organic Framework as a Fluorescent Probe for the Ultrasensitive and Reversible Detection of PO_4^{3-} Ions. *Inorg. Chem.* **2018**, *57*, 10525–10532.
54. Zhou, Z.; Wang, Q. An efficient optical-electrochemical dual probe for highly sensitive recognition of dopamine based on terbium complex functionalized reduced graphene oxide. *Nanoscale* **2014**, *6*, 4583–4587.
55. Ren, M.; Brites, C.D.S.; Bao, S.S.; Ferreira, R.A.S.; Zheng, L.M.; Carlos, L.D. A cryogenic luminescent ratiometric thermometer based on a lanthanide phosphonate dimer. *J. Mater. Chem. C* **2015**, *3*, 8480–8484.
56. Liu, K.; You, H.; Zheng, Y.; Jia, G.; Song, Y.; Huang, Y.; Yang, M.; Jia, J.; Guo, N.; Zhang, H. Facile and rapid fabrication of metal-organic framework nanobelts and color-tunable photoluminescence properties. *J. Mater. Chem.* **2010**, *20*, 3272–3279.
57. Ladol, J.; Khajuria, H.; Sheikh, H.N.; Khajuria, Y. Synthesis and characterization of bi-functional magneto-luminescent Fe_3O_4@SiO_2@$NaLuF_4$:Eu^{3+} hybrid core/shell nanospheres. *J. Chem. Sci.* **2016**, *128*, 1149–1155.
58. Ansari, A.A.; Joselito, P, L.; Aslam Manthrammel, M. Synthesis, structural, and photoluminescence studies of LaF_3:Pr, LaF_3:Pr@LaF_3, and LaF_3:Pr@LaF_3@SiO_2 nanophosphors. *J. Aust Ceram. Soc.* **2018**, *54*, 493–500.